Turkish Journal of Electrical Engineering & Computer Sciences

http://journals.tubitak.gov.tr/elektrik/

Research Article

Turk J Elec Eng & Comp Sci
(2018) 26: 644 – 654

doi:10.3906/elk-1706-238

Presentation of a multilayer nanosensor for gas detection by palladium-membrane with emphasis on hydrogen gas

Ali Mohammad NOORIAN[1], **Mahdi SADEGHI**[2], **Hassan RASOOLI SAGHAI**[2,*]
[1]Faculty of Engineering and Technology, Shomal University, Amol, Mazandaran, Iran
[2]Department of Electrical Engineering, Tabriz Branch, Islamic Azad University, Tabriz, Iran

Received: 20.06.2017 • **Accepted/Published Online:** 20.12.2017 • **Final Version:** 30.03.2018

Abstract: Hydrogen gas sensors, based on palladium membranes, have considerable applications in areas such as industry, aerospace, and green energy monitoring. In this paper, we propose a surface plasmon resonance nanosensor, in which the main metal sensor is taken to be gold with a thin nanolayer of palladium membrane. The reason we chose palladium is its exceptional property of having high permittivity to hydrogen penetration. In this paper, formation of palladium hydride (PdH_x, where x = H / Pd) is achieved and simulation is provided using Materials Studio software. Based on an intermediate assumption, a semiconductor gold composite layer is used instead of gold, because the composite layer gives higher efficiency. In the final structure, twelve alternating layers of gold and silicon are used (silicon and gold with thicknesses of 0.53 and 13.6 nm, respectively). The proposed structure is simulated under carbon monoxide exposure to analyze its cross-sensitivity to other gases. Finally, the sensor shows higher sensitivity and narrower linewidth under hydrogen exposure compared to carbon monoxide exposure.

Key words: Surface plasmon resonance nanosensor, hydrogen sensor, palladium membrane, angle modulation, gas detection, palladium membrane, nanosensor

1. Introduction

Due to its high accuracy, surface plasmon resonance (SPR) in measurements is one of the most powerful methods that is used extensively in biosensors [1]. The resonance method of measurements has many advantages, in particular high sensitivity. In the late 1970s, the surface plasmon was first used to describe the behavior of thin membranes and to study the processes occurring in metallic boundaries [2]. This physical process was first discovered in the 1920s by Wood, who noticed unnatural diffraction when impinging a polarized light on a mirror using diffraction gratings [3,4]. After that, Fano (1941), Otto (1968), and Kretschmann and Raether (1968) paved the way for plasmonic excitations [5–7]. Many applications of surface plasmon excitations have been made, including computer chip design, diagnosis and curing of cancer, ultrasensitive molecular detectors, and invisibility, which are all possible by considering negative diffraction indices [8]. The fundamental system for SPR measurement is the Kretschmann prism configuration. The angle at which the maximum coupling can happen is related to changes in the characteristics of the excitation light [9]. In this paper, SPR for different sensor designs is analyzed in terms of resonance angle and linewidth. A comparison is then provided, considering the width at half of maximum as well as resolution characteristics.

*Correspondence: h_rasooli@iaut.ac.ir

2. General structure of the sensor

Figure 1 gives the original structure of a sensor in a general setting. After the prism, a thin layer of chromium plate, with a thickness of 1 nm, is used to provide easy adhesiveness between prism and metal. The main metal piece of the sensor is chosen to be gold because of its resistance to environmental factors such as oxidation and chemical reaction. The simulation results show that light absorption becomes high when gold thickness is 40 nm or more. Therefore, the thickness of the gold layer is chosen to be 40 nm.

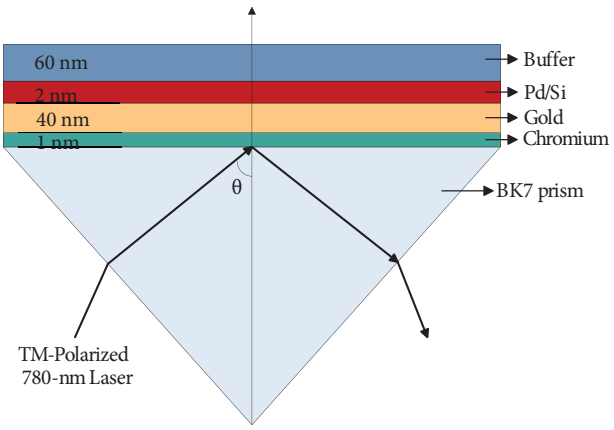

Figure 1. Sensor design used in the simulations, employing Kretschmann surface plasmon resonance (SPR) configuration. In this structure, the thickness of chromium, gold, Pd/Si layers, and buffer are 1 nm, 40 nm, 2 nm, and 60 nm, respectively [10].

After the gold layer, a thin membrane of palladium with a thickness of 2 nm is chosen as the active layer of the sensor. We chose this layer due to its exceptional ability to absorb hydrogen gas [10]. Variations in the optical signal amplitude and resonance wavelength are a function of hydrogen concentration [11]. Additionally, the response of the sensor depends on hydrogen penetration of the metal. Depending on hydrogen concentration, there are two phases of PdH_x, the α-phase and β-phase, under low and high hydrogen concentrations, respectively. Increasing hydrogen concentration causes considerable increase in the palladium lattice constant. The most important parameter in the behavior of the sensor is the phase change [12]. In the α-phase ($x < 1.5\%$), the PdH_x lattice constant increases from 3.890 Å to 3.895 Å, expanding the PdH_x. Since the hydrogen density is low, the volume of the palladium lattice can be reversed. In contrast, if the density of the hydrogen is high ($x > 60\%$), then PdH_x will be converted to the beta phase and will increase the lattice parameter to 4.25 Å. The change resulting from the palladium volume expansion in the beta phase is irreversible. The medium density region ($1.5\% < x < 60\%$) between the alpha and beta phases is called the coexistence region [13]. This region of the density is satisfied at room temperature. By increasing the temperature, the medium density region diminishes (see Figure 2). In Figure 2, the PdH_x layer is used for sensing using Materials Studio software, whose results are used for the final simulation. The last layer of the structure is the buffer. Having hydrogen will cause internal variations in the palladium, including inflammation and fracture in the palladium membrane. There are two common methods to avoid this problem: using alloys of palladium with other metals or using a buffer layer to keep the stability of the palladium structure. In this paper, we will concentrate on the latter [14]. To do that, a single frequency light source with a wavelength of 780 nm and a prism are used for the analysis of the reflected light beam. The reason for using the 780-nm wavelength is that the absorption is maximum due to high plasmonic excitation.

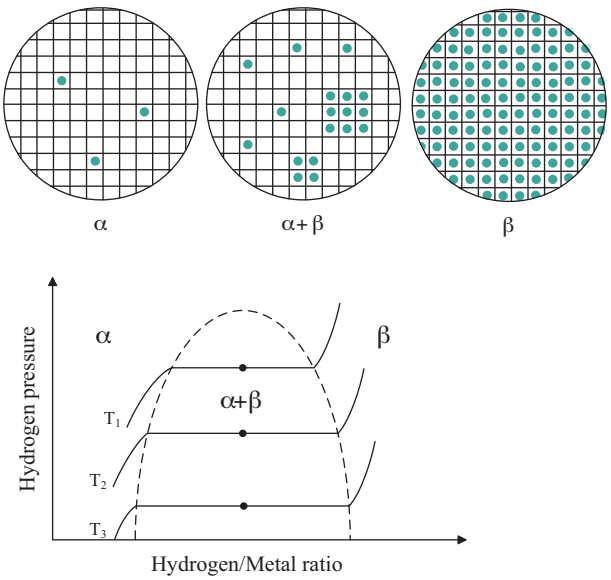

Figure 2. The α- and β-phase formations in the PdH_x. Top: Sketch of the hydride formation process in a metal. The different stages during the hydride formation are α-phase, mixed phase, and fully formed hydride (β-phase). Bottom: Sketch of isotherms showing a plateau at the hydride formation pressure for a given temperature. This plateau increases as the temperature increases [13].

2.1. Idea

The objective of this paper is the optimization and amplification of the decaying radiation field with high absorption efficiency, using the structural change in the sensor. After the injection and penetration of the hydrogen gas in the palladium membrane, and considering the fact that expansion of the palladium will cause changes in the index of refraction in order to achieve the best possible condition, we used multilayers of metal semiconductor (gold and silicon) instead of gold alone, with 6 pairs of alternating layers of gold and silicon. In doing so, we noticed an increase in the sensitivity level of the sensor. The percentage ratio of gold/silicon, considering 40 nm of thickness of 6.13 nm of gold and 0.53 nm of silicon, is 92% to 8%. In doing so, we have obtained the best possible decaying radiation field.

2.2. Equations

Precise mathematical equations are required to implement a particular algorithm of a system. SPR occurs when the unstable vector K_x coincides with the surface plasmon wave vector K_{sp} [1]. Figure 3 shows the SPR configuration of Kretschmann, which we used during the numerical simulations.

The mathematical equations of K_x and K_{sp} are given in Eqs. (1) and (2), respectively:

$$K_x = \frac{2\pi}{\lambda} n_p \sin(\theta), \tag{1}$$

$$K_{sp} = \frac{2\pi}{\lambda} \sqrt{\frac{\varepsilon_m \varepsilon_d}{\varepsilon_m + \varepsilon_d}}, \tag{2}$$

where ε_m, ε_d, and n_p are the complex dielectric constant of metal/dielectric, dielectric complex dielectric constant, and refractive index of prism, respectively. Note that λ is considered to be the wavelength of the

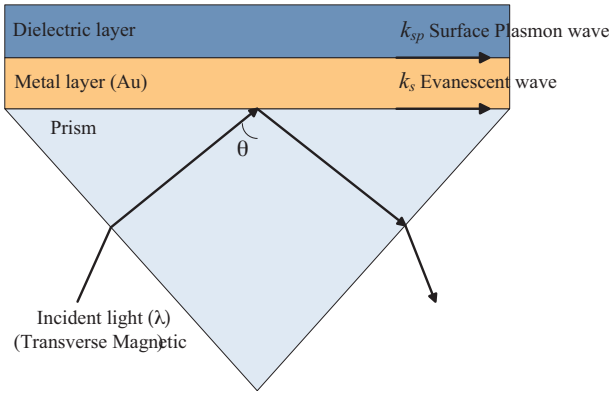

Figure 3. Schematic of Kretschmann SPR configuration [2].

incident light. Eq. (3) shows the functional relationship of the resonance angle dielectric constants:

$$K_x = K_{sp}, \quad \theta_{sp} = \sin^{-1}\sqrt{\frac{\varepsilon_m \varepsilon_d}{\varepsilon_p\left(\varepsilon_m + \varepsilon_d\right)}} \tag{3}$$

Considering the case of resonance, we notice variation in the phase angle and in the reflected light. Both are due to the thickness of the membrane and light constant of the metallic layer. To analyze and design a sensor, two criteria must be considered: metal type and metal thickness [2]. To arrive at a precise mathematical relationship describing the multilayer structure of Figure 4, we need three steps for justification. In the first step, the refraction and reflection of part of the unconventional wave must be considered as a function of the incident wave. In the second, the obtained equations must be converted into an initial matrix for describing the unit transition matrix. In the third step, these operations must be carried out through a medium or channel in order to come up with a unit matrix that describes a behavior of a stack of several mediums.

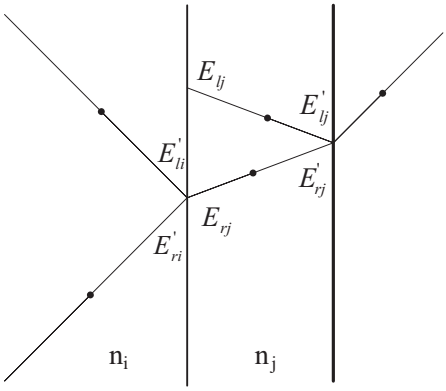

Figure 4. Light reflection and refraction mode, where the direction of the electric field is from the left [15].

Let n_i and n_j be the refraction indices of two different mediums. Then Eqs. (4) and (5) describe the field (E), with its two components on both sides of the medium, as:

$$E'_{ri} = \left(\frac{\rho_{ij}}{\tau_{ij}}\right) E_{lj} + \left(\frac{1}{\tau_{ij}}\right) E_{rj}, \tag{4}$$

$$E'_{li} = \left(\frac{1}{\tau_{ij}}\right) E_{lj} + \left(\frac{\rho_{ij}}{\tau_{ij}}\right) E_{rj}, \tag{5}$$

where E'_{ri}, E'_{li}, E_{lj}, E_{rj}, ρ_{ij}, and τ_{ij}, are electric field from left to right, electric field on the left alone, reflected electric field from right to left, penetration electric field through the Jth medium, reflection coefficient, and transition coefficient, respectively. Now, considering EM polarized light, we can compute τ_{ij} and ρ_{ji} for electric field E from Eqs. (6) and (7):

$$\tau_{ij} = \frac{2\left(\tilde{n}_i \,/\, \tilde{n'}_j\right)}{1 + b}, \tag{6}$$

$$\rho_{ij} = \frac{1 - b}{1 + b}, \tag{7}$$

$$b = \left(\frac{\tilde{n}_i}{\tilde{n}_j}\right)^2 \left(\frac{k_{z,j}}{k_{z,i}}\right), \tag{8}$$

and then write the matrix form of Eqs. (4) and (5) as:

$$\begin{pmatrix} E'_{li} \\ E'_{ri} \end{pmatrix} = \frac{1}{\tau_{ij}} \begin{pmatrix} 1 & \rho_{ij} \\ \rho_{ij} & 1 \end{pmatrix} \begin{pmatrix} E_{lj} \\ E_{rj} \end{pmatrix}, \tag{9}$$

$$E'_i = H_{ij}\, E_j, \tag{10}$$

where H_{ij} is the transfer matrix for the electric field between layers i and j, as shown in Eq. (11):

$$H_{ij} = \frac{1}{\tau_{ij}} \begin{pmatrix} 1 & \rho_{ij} \\ \rho_{ij} & 1 \end{pmatrix}. \tag{11}$$

Similarly (not shown here), a transfer matrix with a phase element $e^{-\beta_j}$ is given in Eq. (12). Phase angle β_j is given in Eq. (13), and n_j, d_j, θ_j, and λ are medium refraction index, layer thickness, incident light angle, and radiation wavelength, respectively.

$$L_j = \begin{pmatrix} e^{-\beta_j} & 0 \\ 0 & e^{-\beta_j} \end{pmatrix} \tag{12}$$

$$\beta_j = \frac{2\pi}{\lambda}\, n_j d_j \cos\left(\theta_j\right) \tag{13}$$

Now, by combining Eqs. (11) and (12), we obtain the complete matrix operator for the multilayer stack, as in Eq. (14).

$$H_{12}L_2H_{23}L_3 \ldots H_{N-1,N}L_{N-1} = S_{1N} = \begin{pmatrix} S_{11} & S_{12} \\ S_{21} & S_{22} \end{pmatrix} \tag{14}$$

Using Eq. (15), which is the ratio of the elements of the second column, we conclude that the SPR is dependent on the type of material, layer thickness, and angle of incident light [15].

$$R = \left|\frac{S_{12}}{S_{22}}\right|^2 \tag{15}$$

2.3. Important sensitivity parameters

2.3.1. Full width at half maximum (FWHM)

A function of the difference between two values of an independent variable is defined. The value of the dependent variable is equal to the FWHM value of the defined function. To achieve maximum sensitivity and minimize the reflection angle, it is preferable to maximize the reflection slope as a function of the incident light beam (see Figure 5) [15]. The width of the curve is dependent on the resonance that is, in turn, largely dependent on the dielectric constant of the metal. In general, the small real part and large imaginary part of the dielectric constant will result in the minimum angle of reflection and a narrower curve [16].

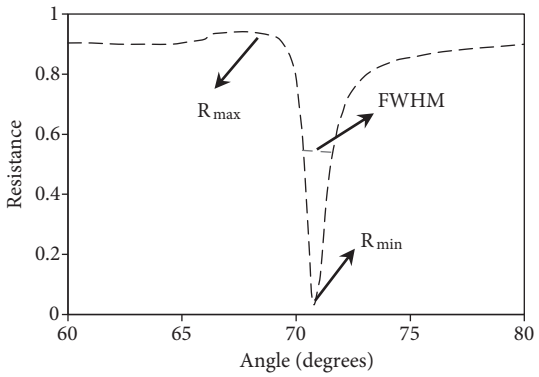

Figure 5. Reflection curve of SPR versus incident angle [12].

2.3.2. Resolution

Resolution is defined in Eq. (16), where R_{Max} and R_{Min} are the maximum and minimum reflection values, respectively, and FWHM is the full width at half of the maximum [17]:

$$SM = Resolution = \frac{R_{Max} - R_{Min}}{FWHM}, \tag{16}$$

where SM is the intrinsic susceptibility of the sensor.

3. Simulation

Refractive indices, extinction coefficients, and thicknesses used in the simulation are given in the Table. First PdH_x is simulated using Materials Studio. For the required modeling for the simulation, we considered Accelrys Materials Studio 6.0. Second, we optimized the palladium surface and injected hydrogen gas into the cubic FCC. We then computed the refractive index (N) and absorption value (K) for the 780-nm wavelength. In Figure 6, the molecular structure for the simulation is shown. The refractive index for a thin PdH_x is computed and given by the complex number N = 1.1962–5.154 i. To do that, the simulation was carried out without palladium hydride, as shown in Figure 7. In the next step, the simulation is performed by injecting hydrogen gas into a thin palladium membrane. The best possible result for the SPR is to consider a 14-layer structure [18]. For this structure, one layer of chromium and one layer of PdH_x, along with 12 layers of alternating gold and silicon, were considered. The ratio of the gold to the silicon was taken to be 6.13/0.53. The final simulation results for a combination of 3, 4, 14, and 16 layers are depicted in Figure 8.

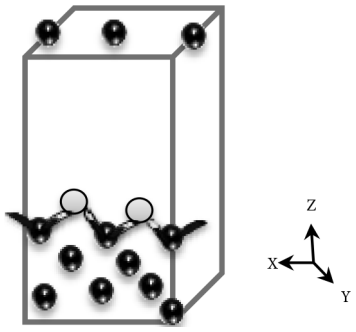

Figure 6. Simulation using Materials Studio.

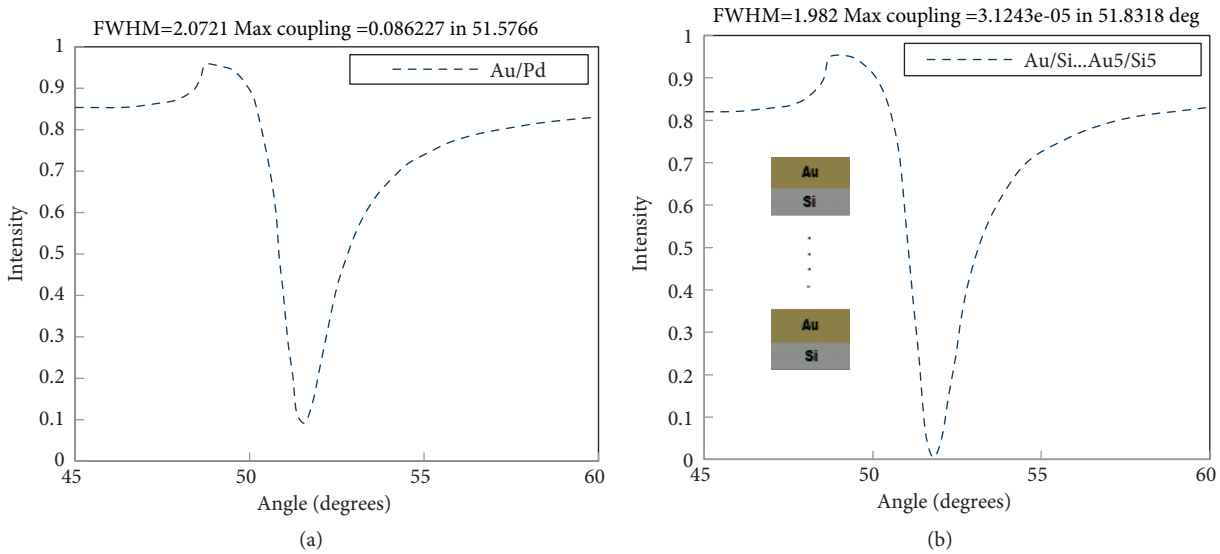

Figure 7. (a) Simulation of primary cell in the presence of PdH_x. (b) Simulation of 12-layer sensor intensity.

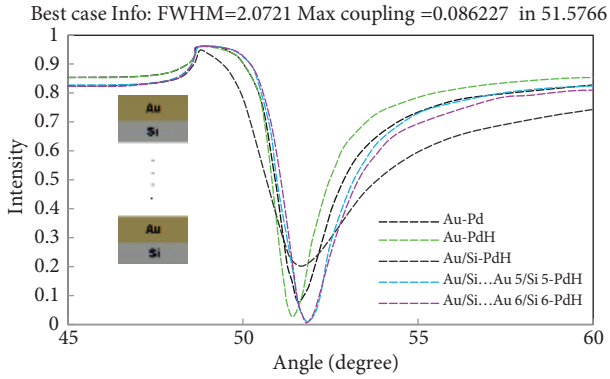

Figure 8. Simulation of sensor intensity using 5 different materials.

Our concern for the simulations of the Pd-H and Pd-CO structures in Materials Studio is to provide an approximate model and evaluate the refraction index along with the absorption coefficient of these two structures after the formation of a composite structure, i.e. the penetration of two different gases into the palladium layer. Based on the effective intermediate assumption theorem, the reason for choosing a silicon semiconductor in

Table. Optical characteristics of 780-nm wavelength.

Material	Refractive index (n)	Extinction coefficient (k)	Thickness
BK 7 prism	1.77	0	-
Chromium	1.77	0	1 nm
Gold	0.17	4.93	36.8 nm
Si	3.71	0.0077	3.2 nm
PdH	1.1962	5.1540	2 nm
NaF buffer (sodium fluoride)	1.3	0	10 nm

the sensor structure is due to the better results of silicon in comparison to other semiconductors. However, according to Figure 9, the results are the same for Si and GaAs semiconductors. Because of the abundance of silicon semiconductors and their ease of use in the chip industry, this paper uses a silicon semiconductor.

3.1. Analysis of width at half of the maximum with respect to the symmetric/nonsymmetric number of layers

Figure 10 shows the simulation results for a multilayer sensor structure, where the blue color represents multilayer symmetric thickness and the dark color represents multilayer asymmetric thickness. As the number of the layers increases up to 12 layers, the FWHM gets narrower (wider) for a symmetrical (nonsymmetrical) structure. Beyond 12 layers, the FWHM does not change and it stays constant as the number of layers further increases.

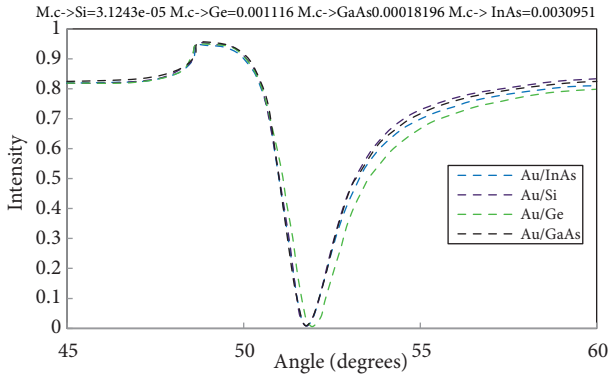

Figure 9. Simulation of sensor intensity for 4 different semiconductor materials.

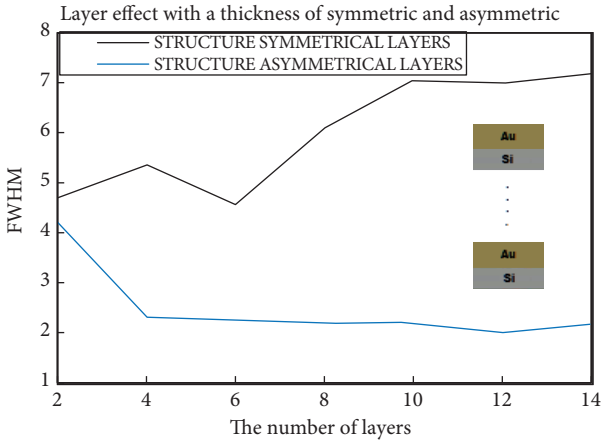

Figure 10. Symmetric/asymmetric thickness effects of multilayer gold-silicon sensor.

3.2. Investigation of the resolution with respect to the symmetric/nonsymmetric number of layers

The resolution and clarification of the sensor in the SPR curve are other sensitivity criteria for sensors. The results of the simulation considering symmetric/asymmetric thickness are shown in Figure 11. As can be seen from this figure, considering the 12-layer gold-silicon symmetric thickness, we notice the highest resolution. For a similar number of layerings with nonsymmetric thickness, the resolution is the lowest.

3.3. Investigation of the effects of other gases

In order to study the response of our structure to the other gases, we consider carbon monoxide gas. With the injection of carbon monoxide gas onto the palladium surface, according to Figure 12, and performing a simulation with Material Studio, we obtain the refraction coefficient of 2.3950–2.8382 i for a wavelength of 780 nm.

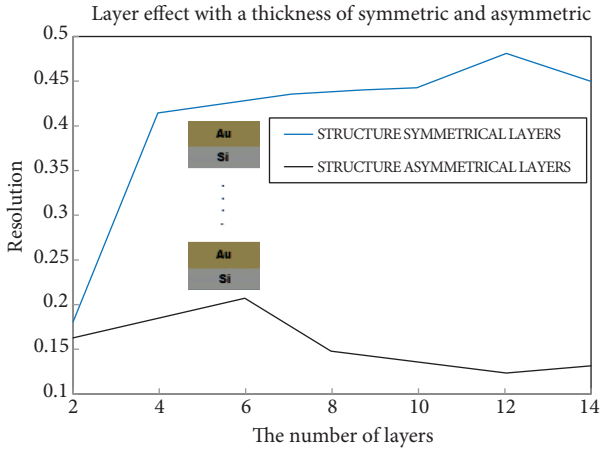

Figure 11. Resolution for symmetric/asymmetric structures.

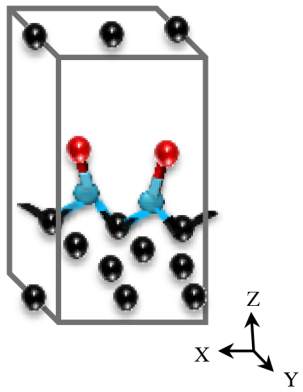

Figure 12. Penetration of carbon monoxide gas molecules into the palladium surface.

3.4. Simulation of the effects of carbon monoxide gas on the main sensor structure

The results of the simulation are shown in Figure 13, where the sensitivity parameters drop considerably. Comparing the simulations for both PdH and PdCO structures, the best results were achieved from PdH_x, with the parameters having a width at which the maximum falls by half. The results are shown in Figure 13.

With respect to the software, all computations were carried out using Castep. The sampling simulation in the software is based on the DFT model, which consists of the following steps:

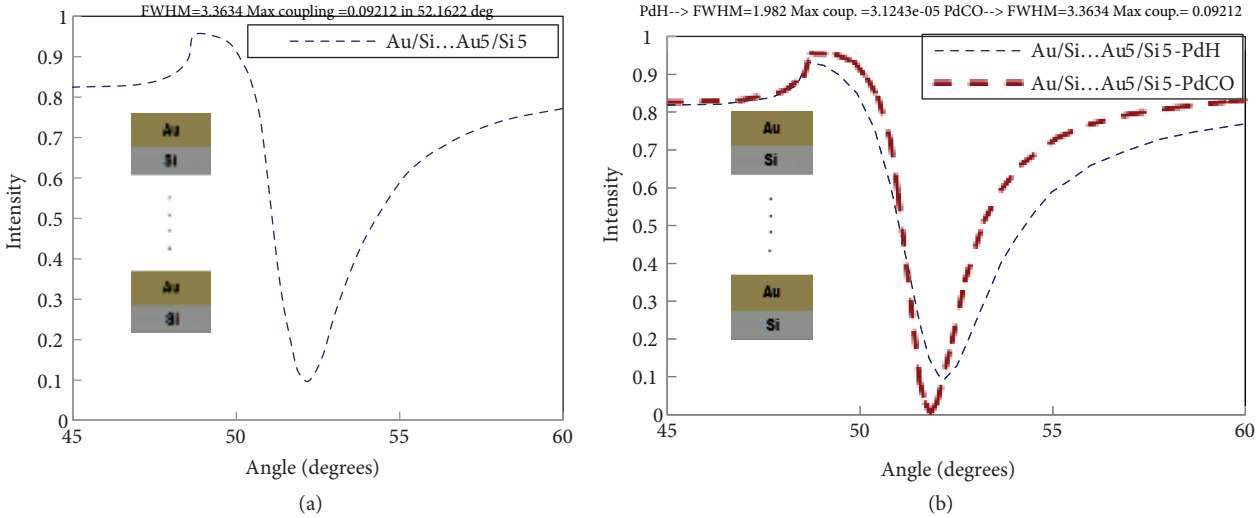

Figure 13. (a) Output of the sensor structure due to carbon monoxide gas effects. (b) Output of the sensor structure for both hydrogen and carbon monoxide gases.

1) Consideration of a layer of palladium with a certain thickness in order to optimize the layer;

2) Adding hydrogen atoms to the palladium layer for simulation of Pd-H;

3) Creation of the C-O structure, optimization, and, finally, penetration of monoxide gas in the layer of palladium;

4) Eventually, analysis of the obtained structure for 780-nm wavelength for refraction index along with absorption.

4. Conclusion

To calculate the refraction index, we used the effective intermediate assumption theorem for the sensor with SPR. The angle modulation with variations in the thickness of the thin membrane was considered. We noticed a reduction in the maximum reflection as a function of the increase in the membrane thickness. According to the different numerical results, we conclude that the gold-silicon membrane thickness is one of the most important parameters for obtaining the highest sensitivity in the sensor configurations. In the simulation of the geometry without the multilayer structure, we showed a poor reaction of the system structure to the PdH_x. We then considered the multilayer structure using the effective intermediate assumption theorem in order to obtain the highest decaying light intensity. In other words, the absorption of light with SPR was noticed. The intensity considering the 12-layer structure was the least. This result was obtained because of the multilayer structure of the silicon semiconductor, with gold with 6 pairs of layers having 8% : 92% silicon : gold ratio and 40 nm of total multilayer thickness. The final composite structure for another type of gas (carbon monoxide) was studied, and we noticed that the maximum coupling at 52.16 was 0.09212. Furthermore, we investigated the most important sensitivity parameters with width at half of the maximum value and with high resolution. We noticed that the 12 alternating layers of gold-silicon composite structure showed a resolution coefficient of 0.4 for symmetric structure and 0.1 for asymmetric structure resolution. We performed the same investigation for carbon monoxide and again obtained the same result of 0.1. Thus, we conclude that the simulated sensor device is much more sensitive to hydrogen than to carbon monoxide, making it selective to hydrogen over carbon monoxide.

References

[1] Pan M. Using multiple layers and surface roughness control for improving the sensitivity of SPR sensors. MSc, Birmingham University, Birmingham, UK, 2009.

[2] Gwon HR, Lee SH. Spectral and angular responses of surface plasmon resonance based on the Kretschmann prism configuration. Mater T 2010; 51: 1150-1155.

[3] Wood RW. On a remarkable case of uneven distribution of light in a diffraction grating spectrum. Philos Mag 1902; 4: 269-275.

[4] Wood RW. Remarkable spectrum from a diffraction grating. Philos Mag 1912; 23: 310-317.

[5] Fano U. The theory of anomalous diffraction gratings and of quasi-stationary waves on metallic surfaces (Sommerfield's waves). J Opt Soc Am 1941; 31: 213-222.

[6] Otto A. Excitation of nonradiative surface plasma waves in silver by the method of frustrated total reflection. Z Phys 1968; 216: 398-410.

[7] Kretschmann E, Raether H. Radiative decay of non-radiative surface plasmons excited by light. Z Naturforsch 1968; 23: 2135-2136.

[8] Trügler A. Optical properties of metallic nanoparticles. PhD, Graz University, Graz, Austria, 2011.

[9] Earp RL. Multiwavelength surface plasmon resonance sensor designs for chemical and biochemical detection. PhD, Virginia Polytechnic Institute, Blacksburg, VA, USA, 1998.

[10] Yun S, Oyama ST. Correlations in palladium membranes for hydrogen separation: a review. J Membrane Sci 2011; 375: 28-45.

11 Yu Z, Jin L, Chen L, Li J, Ran Y, Guan BO. Microfiber Bragg grating hydrogen sensors. IEEE Photonic Tech L 2015; 27: 2575-2578.

[11] Perrotton C, Westerwaal RJ, Javahiraly N, Slaman M, Schreuders H, Dam B, Meyrueis P. A reliable, sensitive and fast optical fiber hydrogen sensor based on surface plasmon resonance. Opt Express 2013; 21: 382-390.

[12] Wadell C, Syrenova S, Langhammer C. Nanoplasmonic hydrogen sensing. SPIE 2014; 9163: 1-13.

[13] Strohfeldt N, Tittl A, Giessen H. Long-term stability of capped and buffered palladium-nickel thin films and nanostructures for plasmonic hydrogen sensing applications. Opt Mater Express 2013; 3: 194-204.

[14] Poulsen MG. Investigation of the Feasibility of SPR as a Method for Detection of Troponin-I by Antibody Binding for Whole Blood Analysis. Aalborg, Denmark: Aalborg University, 2010.

[15] Tudos AJ, Schasfoort RBM. Handbook of Surface Plasmon Resonance. 1st ed. Cambridge, UK: RSC Publishing, 2008.

[16] Bahrami F, Alam MZ, Aitchison JS, Mojahedi M. Dual polarization measurements in the hybrid plasmonic biosensors. Plasmonics 2012; 8: 465-473.

[17] Ghatei Khiabani Azar H, Rasouli Saghai H. Manipulating frequency-dependent diffraction, the linewidth, center frequency and coupling efficiency using periodic corrugations. Opt Quant Electron 2016; 48: 464.